Cryo-EM structure of a Marseilleviridae virus particle reveals a large internal microassembly

Kenta Okamoto, Naoyuki Miyazaki, Hemanth K N Reddy, Max F Hantke, Filipe R N C Maia, Daniel S D Larsson, Chantal Abergel, Jean-Michel Claverie, Janos Hajdu, Kazuyoshi Murata, et al.

Virology 516 (2018) 239–245

Contents lists available at ScienceDirect

Virology

journal homepage: www.elsevier.com/locate/virology

Cryo-EM structure of a *Marseilleviridae* virus particle reveals a large internal microassembly

Kenta Okamoto[a,*,1], Naoyuki Miyazaki[b,1], Hemanth K.N. Reddy[a], Max F. Hantke[a], Filipe R.N.C. Maia[a], Daniel S.D. Larsson[a], Chantal Abergel[c], Jean-Michel Claverie[c,d], Janos Hajdu[a,e], Kazuyoshi Murata[b,*], Martin Svenda[a]

[a] Laboratory of Molecular Biophysics, Department of Cell and Molecular Biology, Uppsala University, Husargatan 3 (Box 596), SE-75124 Uppsala, Sweden
[b] National Institute for Physiological Sciences (NIPS), Okazaki, Aichi, 444-8585 Japan
[c] Structural and Genomic Information Laboratory, UMR 7256 (IMM FR 3479) Centre National de la Recherche Scientifique & Aix-Marseille University, Marseille 13288, France
[d] Assistance Publique des Hôpitaux de Marseille, La Timone, 13005 Marseille, France
[e] Institute of Physics AS CR, v.v.i., Na Slovance 2, 18221 Prague 8, Czech Republic

ARTICLE INFO

Keywords:
Cryo-electron microscopy
Tomography
Melbournevirus
Marseilleviridae
NCLDV
Virus
Structure
Capsid
Protein complex
Amoeba

ABSTRACT

Nucleocytoplasmic large DNA viruses (NCLDVs) blur the line between viruses and cells. Melbournevirus (MelV, family *Marseilleviridae*) belongs to a new family of NCLDVs. Here we present an electron cryo-microscopy structure of the MelV particle, with the large triangulation number T = 309 constructed by 3080 pseudo-hexagonal capsomers. The most distinct feature of the particle is a large and dense body (LDB) consistently found inside all particles. Electron cryo-tomography of 147 particles shows that the LDB is preferentially located in proximity to the probable lipid bilayer. The LDB is 30 nm in size and its density matches that of a genome/protein complex. The observed LDB reinforces the structural complexity of MelV, setting it apart from other NCLDVs.

1. Introduction

Nucleocytoplasmic large DNA viruses (NCLDVs) share genetic and structural traits (Iyer et al., 2001). Comparative genomics of NCLDVs has evoked speculations on the origin of DNA viruses as a distinct domain of life and their role in the evolution of cellular organisms (Abergel et al., 2015; Claverie and Abergel, 2013).

A large variety of icosahedral NCLDVs has to date been isolated from unicellular eukaryotes such as algae and amoeba (Claverie et al., 2009; Dornas et al., 2014; La Scola et al., 2003; Monier et al., 2008; Reteno et al., 2015; Saadi et al., 2013; Santini et al., 2013; Van Etten et al., 1982; Yan et al., 2005). *Marseilleviridae*, including Melbournevirus (MelV) reported in this study, is a recently established family among the large amoebal NCLDVs (Colson et al., 2013; Doutre et al., 2014). They form capsids that vary in size from 190 to 250 nm. The particle architecture and the protein-encoding genes places them taxonomically in a unique family separated from other NCLDVs (Aherfi et al., 2014; Doutre et al., 2015, 2014; Thomas et al., 2011). All these NCLDVs seem to share an evolutionary relationship, albeit complex, based on a core set of conserved genes such as the major capsid protein, the DNA polymerase and other common enzymes, and their virion structures (Iyer et al., 2001; Koonin and Yutin, 2010; Yutin and Koonin, 2012).

Structural studies of the NCLDV particles are important for understanding their assembly, mechanism of cell entry, and evolution. Electron cryo-microscopy (cryo-EM) structures of viral particles of NCLDVs have shown that some of the large capsids adopt regular icosahedral lattices with large triangulation numbers (T-number) built up by an evolutionary related major capsid protein (MCP) (Andreani et al., 2017; Ang and Schaposnik, 2017; Klose et al., 2010, 2016; Kuznetsov et al., 2010; Sinkovits and Baker, 2010; Xiao et al., 2005, 2017, 2009; Yan et al., 2005, 2000). The MCP consists of two jellyroll motifs, similar to many other dsDNA viruses, and the pseudo-hexametric capsomer unit is composed of a trimer of MCPs. The capsids of these large viruses tend to disintegrate into pentagonal and triangular units (penta-symmetrons and trisymmetrons) where the triangular units do not

* Corresponding authors.
E-mail addresses: kenta.okamoto@icm.uu.se (K. Okamoto), kazum@nips.ac.jp (K. Murata).
[1] These authors contributed equally to this work.

https://doi.org/10.1016/j.virol.2018.01.021
Received 17 November 2017; Received in revised form 24 January 2018; Accepted 25 January 2018

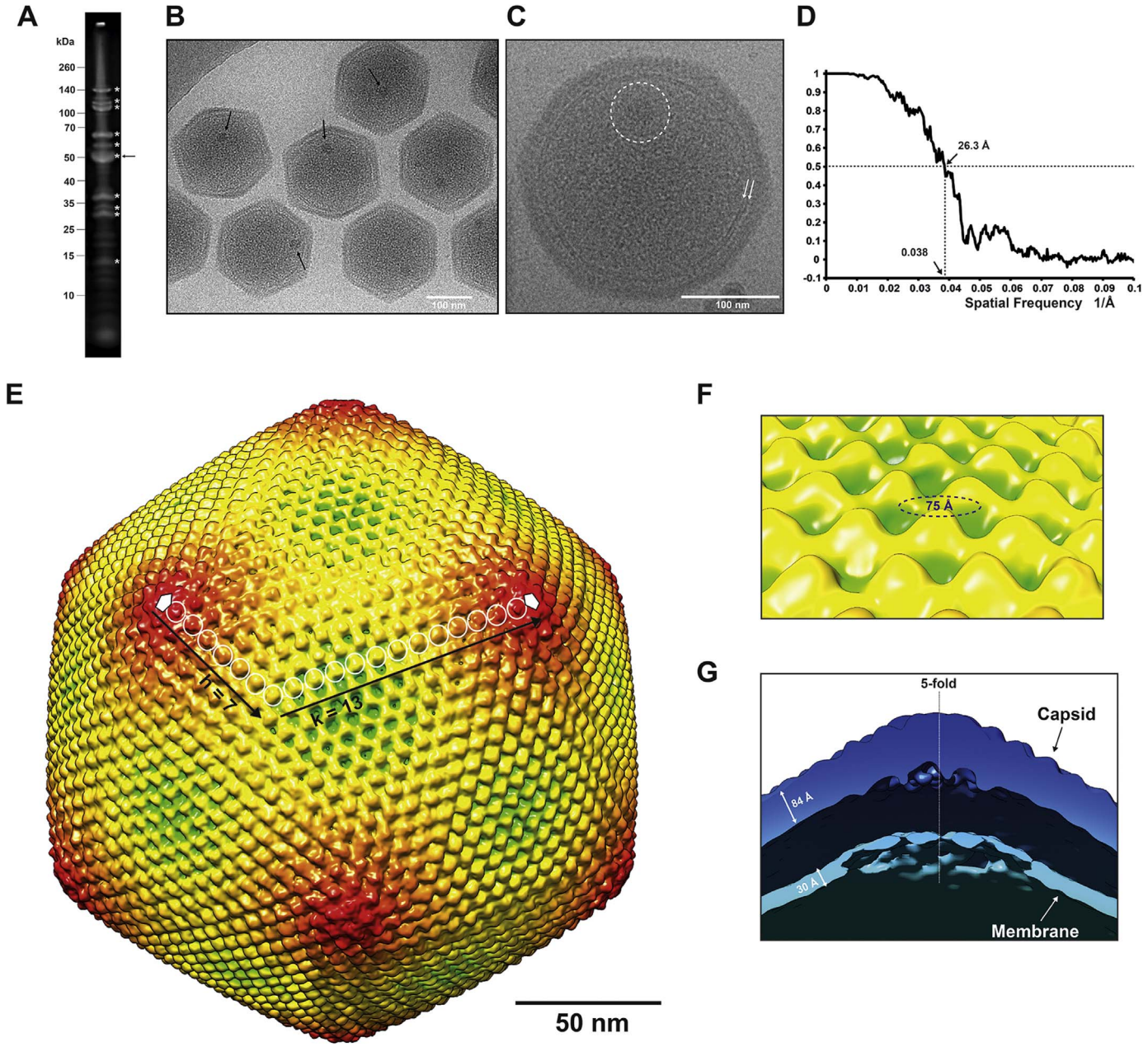

Fig. 1. Images of cryo-frozen MelV particles and single particle 3D reconstruction. A) A SDS-page gel of the purified virions used for the single particle analysis. The arrow indicates the band of the conserved MCP. White asterisks indicate 10 abundant major proteins. B, C) Raw images of the MelV. Black arrows in B) and white dotted circle in C) indicate LDBs. White arrows in C) indicate the double-layered membrane. D) Fourier shell correlation between two independently reconstructed half sets of images with an inner mask applied. The resolution estimated by a 0.5 cutoff is 26.3 Å. E) The T = 309 capsid lattice of the MelV. Surface plot of the reconstructed 3D structure at an isodensity contour level of 2.0 σ coloured according to the distance from the center of the virus particle (green < 1050 Å, yellow < 1070 Å, red < 1200 Å. The T-number was determined by counting the number of the protrusions in the lattice (black arrows and white circles). Each protrusion represents a capsomer. With h = 7 and k = 13 it corresponds to T = 309. F) Close-up view of the surface protrusions that are the tips of the pseudo-hexagonal capsomers. G) A cross-section of the 3D density perpendicular to a 5-fold axis. The capsid and membrane structures were rendered at an isodensity contour level of 1.0 σ using a cryo-EM model at the resolution of 35.0 Å without applying any inner mask.

necessarily correspond to the triangular facets of the approximately icosahedral capsid (Nandhagopal et al., 2002; Wrigley, 1969). In addition to these regular capsid traits of the NCLDVs, some NCLDVs possesses unique features such as the stargate, long fibers and internal multi-layered membranes of the Mimivirus particle (Abergel et al., 2015; Arslan et al., 2011; La Scola et al., 2003; Schrad et al., 2017; Xiao et al., 2005, 2009), the unique vertex of the *Paramecium bursaria* Chlorella virus 1 (PBCV-1) particle (Cherrier et al., 2009), and the double-layered capsids of Faustovirus (Klose et al., 2016). Here we present a cryo-EM structure of the MelV particle, displaying unique structural features that set it apart from other NCLDVs.

2. Results

2.1. Identification of structural proteins of the MelV particle

The MelV genome encodes 403 open reading frames. Purified virions contain at least 10 major (abundant) proteins and many minor proteins (Fig. 1A). The most intense band of the SDS-PAGE appears at around 50 kDa (black arrow in Fig. 1A) and is thought to correspond to the MCP (predicted molecular weight of 52.4 kDa). The purified virus particles were also analyzed by tandem mass spectrometry (MS)-based proteomics analysis after 9 M urea treatment (Supplementary Table S1 and S1-2). The MCP was identified as well as histone-like or histone-

related proteins, several putative viral enzymes (a cysteine peptidase, helicases, AAA-family ATPases, thioredoxins, putative serine/threonine protein kinases, an uracil-DNA glycosylase, a putative glycosyltransferase, a mannosyltransferase, an amine oxidase, a putative ribonuclease and a sulfhydryl oxidase) and many functionally uncharacterized proteins were identified. We also identified some putative membrane proteins.

2.2. Cryo-EM and single particle analysis (SPA)

The icosahedral MelV particle is ~ 230 nm in diameter (Fig. 1B). An approximately spherical double layer, assumed to be an inner membrane, can be observed beneath the icosahedral capsid (white arrows in Fig. 1C). Almost all particles show a dense interior, which indicates that most of them are filled with the viral genome and proteins. All particles clearly display an interior spot, approximately 30 nm in diameter that is much denser than the rest of the interior. The shape of the large and dense body (LDB) does not seem to be spherical and the location within the particle is not fixed, but it is consistently present (black arrows in Fig. 1B and a white circle in Fig. 1C). Bubblegram imaging was used to visualize an inner body of the large bacteriophage ϕKZ, showing that it has a chemically distinct radiation response, different from protein components (Wu et al., 2012). The LDB of MelV did not show a specific radiation damage profile (Supplementary Fig. S1).

In total, 7005 cryo-EM projection images of virus particles were used for the 3D reconstruction. The final resolution was estimated to be 26.3 Å by calculating the Fourier shell correlation (FSC) between two independent half-sets and using a 0.5 cutoff (Fig. 1D). The distance between the two farthest 5-fold vertices of the capsid is 232 nm. The capsid surface is covered with ordered protrusions (Fig. 1E, F). Similarly ordered protrusions have previously been reported in the structures of other related NCLDVs at intermediate resolution, and assigned as the pseudo-hexagonal capsomers built up by the conserved trimeric MCP (Nandhagopal et al., 2002; Yan et al., 2005). The ordered protrusions of the MelV particle are approximately 75 Å in diameter (Fig. 1F), which is in the range of the capsomer size of other NCLDVs (Nandhagopal et al., 2002). The approximate thicknesses of the capsid and the membrane are 84 Å and 30 Å, respectively (Fig. 1G). The internal membrane appears to bulge out near the 5-fold axis (Fig. 1G).

2.3. Geometry of the capsid

The allowed T-numbers are defined by the formula $T = h^2 + hk + k^2$ where the integers h and k define the number of lattice points between neighboring vertices (Caspar and Klug, 1962). At the given resolution of the reconstruction, the hexameric capsomers of the MelV particle appear as ordered protrusions (Fig. 1F). Counting the number of capsomers between two neighboring 5-fold vertices (Fig. 1E), we conclude that h = 7, k = 13, and T = 309 for the MelV capsid lattice. The indexing of the capsid lattice was confirmed by comparing the reconstruction with simulated levo or dextro handed lattices, i.e. (h, k) = (7, 13) or (h, k) = (13, 7), respectively (Supplementary Fig. S2). A theoretical analysis of the possible pentasymmetron-trisymmetron models of large NCLDVs was previously reported (Simpson et al., 2003) and later formalized into a set of selection rules (Sinkovits and Baker, 2010). According to the theory, the size of the pentasymmetrons and trisymmetrons correlates with the h and k values used for T-number determination. In the case (h, k) = (7, 13), the lattice consists of pentasymmetrons with 4 capsomer long edges, and trisymmetrons with 16 capsomer long edges, giving 30 and 136 capsomers in each pentasymmetron and trisymmetron, respectively (Fig. 2 and Table 1). The total number of pseudo-hexagonal capsomers is 3080 (Table 1), which in turn are assembled by 9240 MCPs in the entire capsid lattice.

2.4. Distribution of LDBs analyzed by electron cryo-tomography

Full 3D models of 147 complete virus particles were obtained by electron cryo-tomography (cryo-ET). In these models the LDB appears as a compact object with high density in an off-centered position close to the capsid/membrane (green isosurface in Fig. 3A). Assuming the weak phase approximation (Vulovic et al., 2014), the image intensity is locally proportional to the object density. The density of the LDB is estimated to be around 1.60 g/cm^3, significantly higher than the average density of the vitreous ice (density 0.92 g/cm^3) and the peak density of the capsid (typical protein density 1.36 g/cm^3) (Perlman et al., 1982; Spahn et al., 2000). The rest of the interior regions have a density in the range of 1.10–1.30 g/cm^3 (Fig. 3B). Multiple 3D subtomograms of MelV particles were aligned to the one unique vertex that was the closest to the LDB, and these aligned subtomograms were averaged (Fig. 3C). The delocalization of the LDB consequently blurs its density, but it seems to most commonly be located near the capsid/membrane (Fig. 3C). The 3D probability distribution of the LDB was calculated from the coordinates of the vertices and the LDB (Fig. 3D, E, Movie S1). The majority of the LDBs are located 400 Å from the nearest vertex and 166 Å below the membrane (Fig. 3E), but rarely exactly on the 5-fold axes (Fig. 3D). A small number of LDBs are located near the center of the particles (Fig. 3D).

3. Discussion

An early preliminary reconstruction showed that *Marseilleviridae* form icosahedral particles (Boyer et al., 2009). The present MelV virion reconstruction is the first *Marseilleviridae* structure where it is possible to determine the capsid geometry including the T-number (Fig. 1). Evolution towards larger capsids seems to favor increasing the size of the trisymmetrons rather than the pentasymmetrons (Fig. 2 and Table 1). The pattern is further confirmed by the recently reported Pacmanvirus (h = 7, k = 13) and CroV (h = 7, k = 18) structures (Andreani et al., 2017; Xiao et al., 2017). By keeping the pentasymmetrons fixed, the required adaptations are limited to the trisymmetron size as well as of the interfaces between them. Further studies of other smaller *Marseilleviridae* virions are required to clarify the relationship between the capsid size and the size of the pentasymmetrons and trisymmetrons.

The LDB is clearly a unique feature of MelV (Figs. 1B, C, and 3). No similar interior complex has been reported in the structures of other NCLDVs (Reteno et al., 2015; Xiao et al., 2009; Yan et al., 2005, 2000), while an inner body was found in the virion of the large bacteriophage ϕKZ (Wu et al., 2012). It is surprising that a large 30-nm object, similar in size to a small virus or to a ribosome, is incorporated into a virus particle (Figs. 1B, C and 3). Several giant amoeba viruses episodically form dot-like or interior fibrillar components (Legendre et al., 2014; Philippe et al., 2013), but in MelV every imaged virus particle has such a component. The position of the LDB is not fixed in the virion, however rarely located exactly on the 5-fold axis or near the center of the particle, and seems to be loosely restrained to the proximity of the capsid/membrane (Fig. 3D). This restriction of the LDB localization may be the result of an interaction between the LDB and the membrane. The LDB is estimated to be around 1.2 times denser than the capsid layer of the virus (Fig. 3B). It is however difficult to pack proteins into the LDB in a manner that makes them denser than the capsid lattice. A previous study of bulk cross-linked chromatin fragments (Schwartz et al., 2005) indicated a density of 1.39–1.42 g/cm^3, while the density of cross-linked proteins is ≤1.25 g/cm^3 and the density of free DNA is ≤1.69 g/cm^3. The presence of several histone-like structural proteins based on our result of MS/MS tandem spectroscopy (Supplementary Table S1) encourages the hypothesis that the LDB consists of a nucleoprotein complex. Other *Marseilleviridae* viruses were also reported to express several histone-like proteins (Aherfi et al., 2016; Boyer et al., 2009; Doutre et al., 2014; Erives, 2017). It is however not feasible to pack the

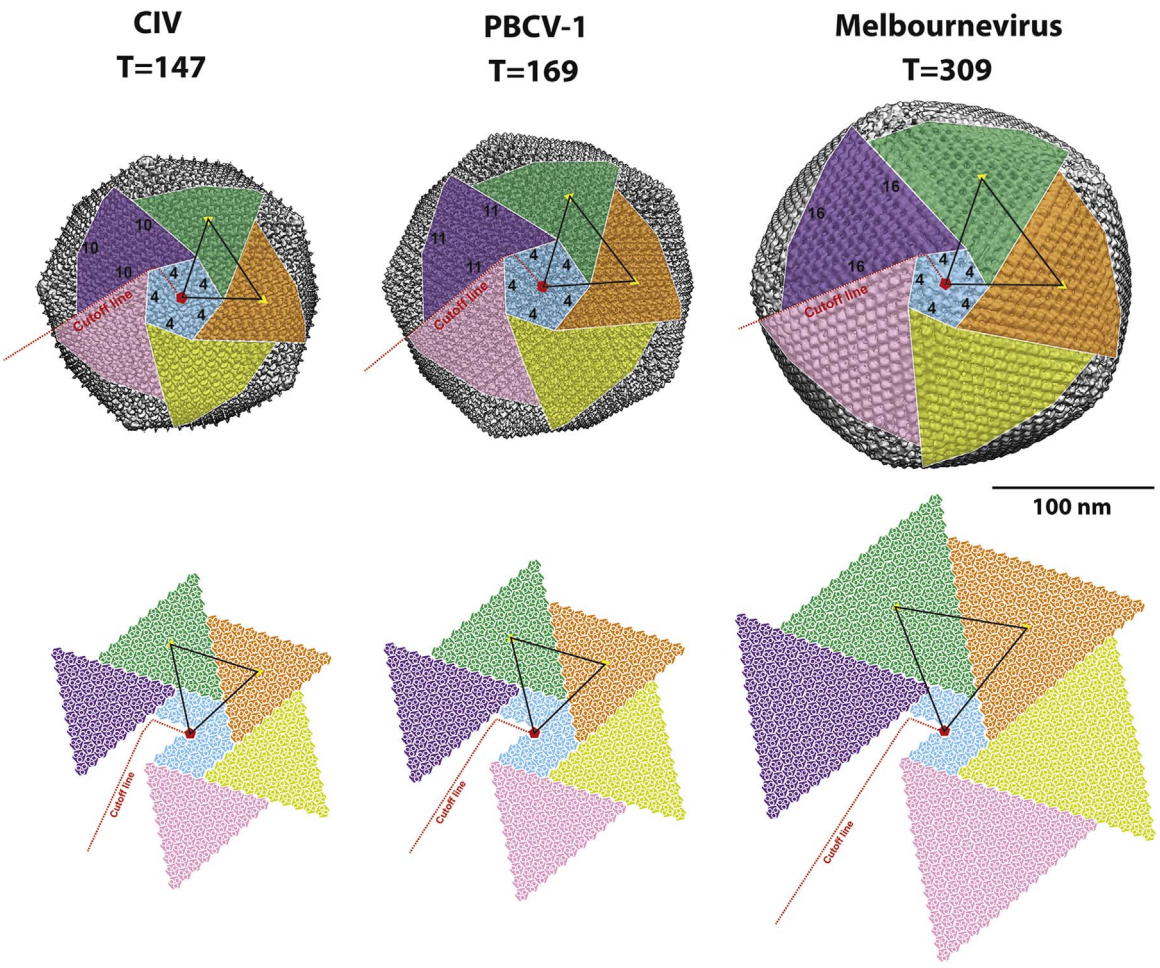

Fig. 2. Trisymmetron and pentasymmetron organization of CIV (EMDB Accession code: 1580), PBCV-1 (EMDB Accession code: 5378) and MelV particles. The number of capsomers on each edge are shown in the figure. Yellow triangles indicate 3-fold axes and a red pentagon a 5-fold axis. Three white circles in every hexagonal capsomer (the bottom expansion plains) indicate the trimeric MCPs that compose the capsomer. Pentasymmetrons with 4 capsomer long edges are common to all virus species.

Table 1
Pentasymmetron and trisymmetron organization in five giant viruses.

	CIV	PBCV-1	PpV01	Faustovirus	MelV
Size					
Diameter nm	185	190	220	240	232
T number					
(h, k)	(7,7)	(7,8)	(7,10)	(7, 12)	(7, 13)
T[*1]	147	169	219	277	309
Hexagonal capsomers					
Trisymmetrons					
Capsomers on each edge (t)[*2]	10	11	13	15	16
The number of capsomers (N_t)[*3]	55	66	91	120	136
Pentasymmetrons					
Capsomers on each edge (p)[*4]	4	4	4	4	4
The number of capsomers (N_p)[*5]	30	30	30	30	30
Total number of capsomers	1460	1680	2160	2660	3080
Pentagonal capsomers					
Total number of capsomers	12	12	12	12	12

[*1] $T = Pf^2 = (h^2 + h*k + k^2)f^2$ [*2] $t = (h + 2k - 1)/2$ [*3] $N_t = [(h+2k)^2-1]/8$ [*4] $p = (h + 1)/2$ [*5] $N_p = [5(h^2-1)]/8$.

entire 369 kbp genome into such a small volume as the LDB, but a part of the genome may be more densely packed or bound to transcription factors or a helicase of the MelV. The density of a eukaryotic ribosome is approximately 1.60 g/cm^3 in free form (Vournakis and Rich, 1971) and the estimated density of the LDB agree with that of the ribosome, although Mollivirus is the only giant amoebal virus that is known to incorporate host ribosomal proteins (Legendre et al., 2015). The host ribosomal protein was not detected in our proteomics analysis of the purified MelV particles. Alternatively, the LDB might be a ribonucleoprotein particle, a complex formed between RNA and RNA-binding proteins. The RNA moiety could be constituted of transcripts (mRNAs) encoding proteins needed to initialize the infectious cycle, ready to be translated in the host cytoplasm. Interestingly, the presence of mRNAs has been detected in the particles of Noumeavirus, another member of the Marseilleviridae family (Fabre et al., 2017). Another possibility is that these mRNA might be complexed with several of the predicted RNA-binding proteins detected in the particle, some of them in high abundance (e.g. helicases, capping enzyme) (Supplementary Table S1). The LDB did not show increased radiation sensitivity compared to the rest of the viral components in bubblegrams (Supplementary Fig. S1). It is difficult to interpret the structure of the LDB in our current limited resolution SPA and tomographic models of the MelV particle. It is challenging to determine the structure of an asymmetric object like the LDB in the dense icosahedral capsid. To better understand the function of the LDB, we would need to have a better understanding of its composition. Ideally one would like to isolate and purify LDB particles, but it has proven to be difficult to break up the rigid capsid while keeping the LDB structure intact. We hope to overcome these difficulties in the future and be able to reveal the function of the unique LDB.

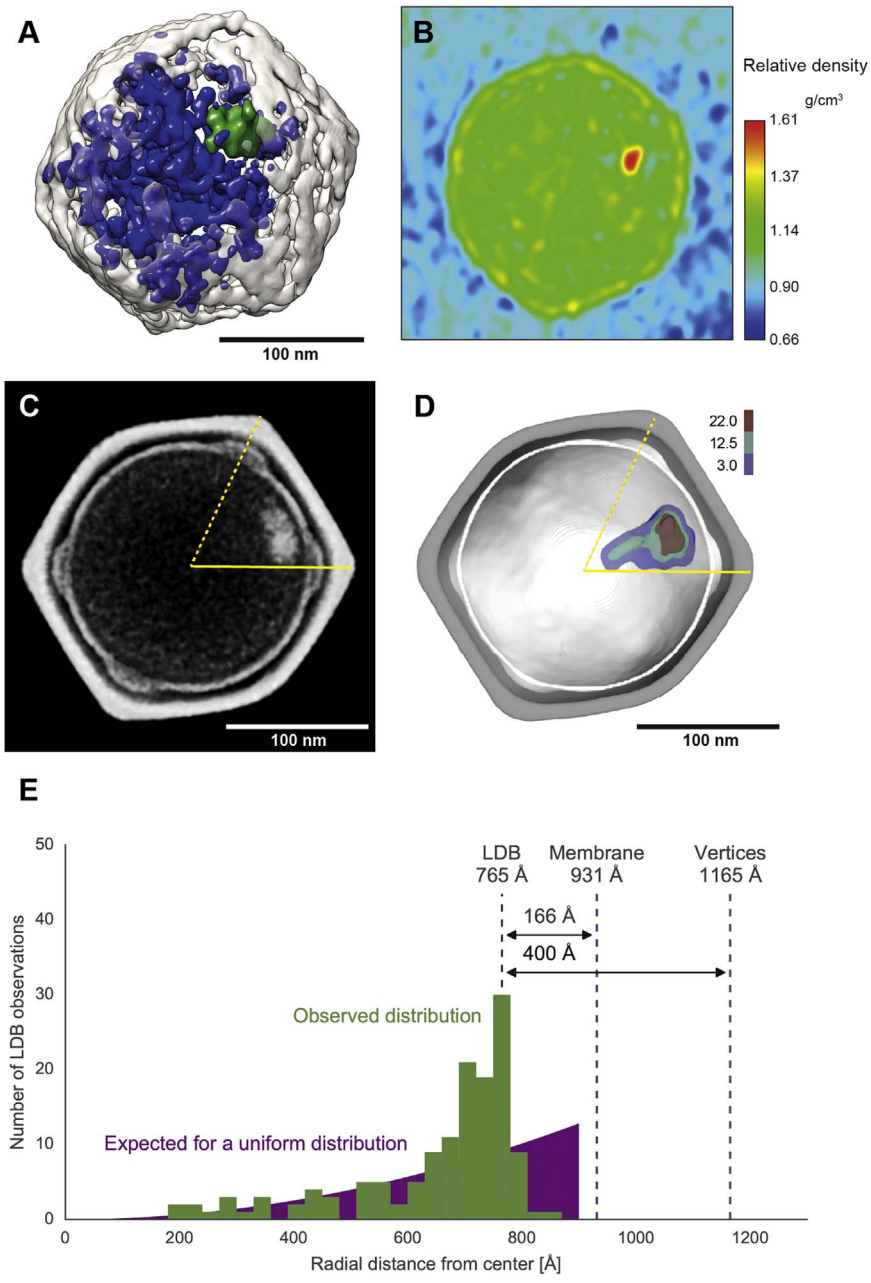

Fig. 3. Cryo-ET 3D reconstruction of the MelV particle, and the intensity and the position of the LDB. A) One of the boxed 3D tomographic reconstructions of the MelV particle. The outer capsid and the membrane, the LDB, and the other interior fragments are shown with white, green, and blue isosurfaces, respectively. B) The relative image intensity in a cross-section of the virion in A), which corresponds to the relative density of the specimen in a weak phase approximation. C) A cross-section of a subtomogram-averaged model of the MelV particle. The LDB is blurred in the model by their variable localizations. D) Spatial distribution of the LDB. The grey and white surfaces indicate the capsid and membrane of the SPA model, respectively. The probability of the spatial distribution (per $Å^3$) of the LDB in the MelV particle is shown in a color gradient (3.0–22.0 × $10^9/Å^3$). C, D) The 5-fold axes are indicated with yellow lines (The closest 5-fold axis of the LDB is indicated with a solid yellow line). E) Distribution of the radial distance of the LDB from the closest 5-fold vertex and the membrane (Green histogram). The purple curve shows the probability of finding the LDB, assuming a uniform distribution in the MelV particle.

4. Materials and methods

4.1. Virus propagation and purification

MelV was propagated in *Acanthamoeba castellanii* cells cultured in PPYG medium (2.0% w/v proteose peptone, 0.1% w/v yeast extract, 4 mM $MgSO_4$, 0.4 mM $CaCl_2$, 0.05 mM $Fe(NH_4)_2(SO4)_2$, 2.5 mM Na_2HPO_4, 2.5 mM KH_2PO_4, and 100 mM sucrose, pH 6.5). The protocol used to purify particles was described previously (Doutre et al., 2014). In short, the infected culture fluid was collected and centrifuged for 10 min at 500 g, 4 °C to remove cell debris. The supernatant was centrifuged for 35 min at 6500 g, 4 °C. The pellet was suspended in 1 mL of PBS buffer. The suspended sample was loaded onto a 10–60% sucrose gradient and centrifuged for 90 min at 6500 g, 4 °C. The concentrated band was collected and dialyzed in PBS. The dialyzed sample was centrifuged for 35 min at 6500 g, 4 °C, and the pellet suspended in PBS was used for further proteomics and cryo-EM analysis.

4.2. Cryo-EM image acquisition and single particle analysis

Purified virus particles were applied onto a holey carbon grid (R1.2/1.3 Quantifoil Micro Tools GmbH, Germany) pretreated by glow-discharge, and plunged-frozen in liquid nitrogen-cooled ethane using a Vitrobot Mark-IV (FEI Company, USA). The ice-embedded sample was observed using a field emission transmission electron microscope (FE-TEM), JEM2200FS (JEOL Ltd. Japan), at 45,317 times detector magnification (3.31 Å/pixel) with an accelerating voltage of 200 kV using a 4k x 4k charge-coupled device (F415, TVIPS GmbH, Germany) and an electron dose of ~20 $e^-/Å^2$. An omega-type energy filter was applied to obtain zero-loss electrons (20 eV slit width). The underfocus values were approximately 1–5 μm. EMAN2 was used for reconstructing the 3D structures from the images (Tang et al., 2007). Virus particles were boxed separately using e2boxer.py (EMAN2). Contrast transfer function (CTF) calculations and amplitude corrections were performed on boxed particles by e2ctf.py (EMAN2), and then manually verified by adjusting the defocus and B-factor values. Several random icosahedral initial

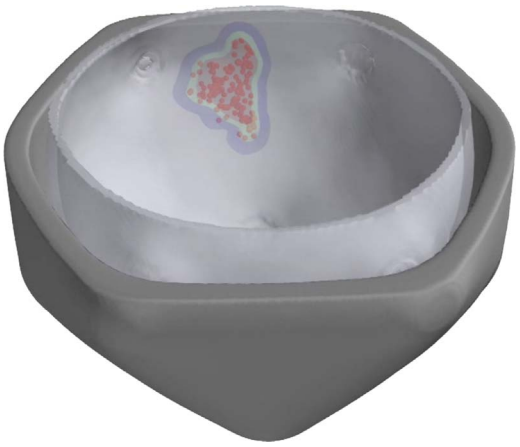

Movie S1. Spatial distribution of the LDB. Supplementary material related to this article can be found online at http://dx.doi.org/10.1016/j.virol.2018.01.021.

models were calculated using class-averaged virus particle images. Initially 1979 virus particles were used for the 3D reconstruction. The signals from the obtained images were weak, so pixel binning was applied when calculating the first model. The pixel size after binning was 6.62 Å/pixel. Icosahedral symmetry was imposed during the 3D refinement. During the reconstruction process, outer radial masking, low-pass filtering, and FSC calculations were applied by the EMAN2 program. The calculations were conducted using a CPU cluster using 100–200 CPU cores per job. After 12 iterative steps of refinement, the first SPA model was generated, which was estimated to have a resolution of 35.0 Å using a FSC resolution cutoff of 0.5. Then, total 7005 particle images without binning (3.31 Å/pixel) and the 35.0 Å starting model were used for reconstructing the final model. After 10 iterative steps of refinement with inner and outer masking, the final SPA 3D model was generated, and the reconstruction was estimated to have a resolution of 26.3 Å with a FSC resolution cutoff of 0.5. The 3D volume of the final model was visualized by UCSF Chimera (Pettersen et al., 2004).

4.3. Tomographic reconstruction and data analysis

Five microliters of the virus sample was mixed with the same amount of 15 nm fiducial marker gold colloids. The specimen was loaded onto a holey-carbon grid (R1.2/1.3 Quantifoil) and plunged-frozen in liquid nitrogen-cooled ethane, and imaged with a FE-TEM, JEOL JEM2200FS, at 24,116 times detector magnification on a 4k x 4k charge-coupled device (TVIPS, F415) with an accelerating voltage of 200 kV. Specimens were tilted from 70° to −70° with 2° angular steps. Images were binned up to 12.11 Å/pixel after collecting the data. The alignment of the images and the final tomograms were calculated by the IMOD software (Kremer et al., 1996) using the colloidal gold fiducial markers. A total of 147 subtomograms of the MelV particle were picked up by EMAN2 (Tang et al., 2007). These particles were low-pass Gaussian filtered by e2proc3d.py (EMAN2). The subsequent post-tomographic image processing was performed using EMAN1 (Ludtke et al., 1999; Tang et al., 2007). The 20 Å low-pass filtered subtomograms were aligned to the SPA model of the MelV particle. These aligned subtomograms were symmetrically rotated to place the LDB to the same asymmetric unit of the icosahedral capsid. The subtomogram-averaged model of the MelV particle was calculated by averaging the oriented subtomograms. To characterize localizations of individual LDBs, the coordinates of the vertices and the interior LDB were determined by the following procedure. First, the final SPA model was rotated to match the orientation of the each low-resolution subtomogram particle. Then, the coordinates of the vertices of the capsid of the SPA model and the densest region within the LDB in the tomographic model were determined by manual selection using the Chimera software (Pettersen et al., 2004). The probability distribution of the LDB was calculated by the coordinates of 147 LDBs positions in the MelV particle applying an isosurface level to these LDB positions.

4.4. Data deposition

The 2.6 nm MelV cryo-EM model was deposited to EMDB (EMD3868).

Acknowledgements

We are grateful to Chuan Xiao, Department of Chemistry, University of Texas at El Paso (UTEP), for a kind discussion of determining T-number. This work was supported by the following agencies: The Swedish Research Council (to J.H., grant number: 628–20081109, 822–2010-6157, 822–2012-5260, and 828–2012-108), the Knut and Alice Wallenberg Foundation (to J.H., grant number: KAW-2011.081), the European Research Council (to J.H., grant number: ERC-291602), the Rontgen-Angstrom Cluster (to J.H., grant number: 349–2011-6488, and 2015–06107), the Swedish Foundation for International Cooperation in Research and Higher Education (STINT) (to J.H. and K.O., grant number: JA2014-5721), The European Regional Development Fund (ELIBIO CZ.02.1.01/0.0/0.0/15_003/0000447) at the European Extreme Light Infrastructure (to J.H.), KAKENHI from the Ministry of Education, Culture, Sports, Science and Technology (MEXT) of Japan (to N.M., grant Number: 25251009), a Grant-in-Aid for Scientific Research on Innovation Area from MEXT of Japan (to K.M., grant Number: 17H05825), and the Collaborative Study Program of National Institute for Physiological Sciences (to K.O., grant Number: 2016-No. 38), the CNRS, Aix-Marseille University and the French National Research Agency (to C.A., grant number: ANR-14-CE14-0023-01). The authors declare no competing financial and non-financial interests.

Author contributions

JH, CA, KO, JMC, KM and MS conceived the experiment. CA and JMC isolated the virus and provided samples. KO, HMKNR, MS performed proteomics studies. KO, NM, MFH, KM and MS performed the cryo-EM studies. KO, NM, MFH, FRNCM, DSDL, CA, JMC, KM and MS analysed the data. All authors read and approved the final manuscript.

Appendix A. Supporting information

Supplementary data associated with this article can be found in the online version at http://dx.doi.org/10.1016/j.virol.2018.01.021.

References

Abergel, C., Legendre, M., Claverie, J.M., 2015. The rapidly expanding universe of giant viruses: mimivirus, pandoravirus, pithovirus and mollivirus. FEMS Microbiol. Rev. 39, 779–796.

Aherfi, S., Colson, P., La Scola, B., Raoult, D., 2016. Giant viruses of amoebas: an update. Front. Microbiol. 7, 349.

Aherfi, S., La Scola, B., Pagnier, I., Raoult, D., Colson, P., 2014. The expanding family marseilleviridae. Virology 466–467, 27–37.

Andreani, J., Khalil, J.Y.B., Sevvana, M., Benamar, S., Di Pinto, F., Bitam, I., Colson, P., Klose, T., Rossmann, M.G., Raoult, D., La Scola, B., 2017. Pacmanvirus, a new giant icosahedral virus at the crossroads between asfarviridae and faustoviruses. J. Virol. 91.

Ang, K.S., Schaposnik, L.P., 2017. On the geometry of regular icosahedral capsids containing disymmetrons. J. Struct. Biol. 197, 340–349.

Arslan, D., Legendre, M., Seltzer, V., Abergel, C., Claverie, J.M., 2011. Distant mimivirus relative with a larger genome highlights the fundamental features of Megaviridae. Proc. Natl. Acad. Sci. USA 108, 17486–17491.

Boyer, M., Yutin, N., Pagnier, I., Barrassi, L., Fournous, G., Espinosa, L., Robert, C., Azza, S., Sun, S., Rossmann, M.G., Suzan-Monti, M., La Scola, B., Koonin, E.V., Raoult, D., 2009. Giant Marseillevirus highlights the role of amoebae as a melting pot in emergence of chimeric microorganisms. Proc. Natl. Acad. Sci. USA 106, 21848–21853.

Caspar, D.L., Klug, A., 1962. Physical principles in the construction of regular viruses.

Cold Spring Harb. Symp. Quant. Biol. 27, 1–24.
Cherrier, M.V., Kostyuchenko, V.A., Xiao, C., Bowman, V.D., Battisti, A.J., Yan, X., Chipman, P.R., Baker, T.S., Van Etten, J.L., Rossmann, M.G., 2009. An icosahedral algal virus has a complex unique vertex decorated by a spike. Proc. Natl. Acad. Sci. USA 106, 11085–11089.
Claverie, J.M., Abergel, C., 2013. Open questions about giant viruses. Adv. Virus Res. 85, 25–56.
Claverie, J.M., Grzela, R., Lartigue, A., Bernadac, A., Nitsche, S., Vacelet, J., Ogata, H., Abergel, C., 2009. Mimivirus and Mimiviridae: giant viruses with an increasing number of potential hosts, including corals and sponges. J. Invertebr. Pathol. 101, 172–180.
Colson, P., Pagnier, I., Yoosuf, N., Fournous, G., La Scola, B., Raoult, D., 2013. "Marseilleviridae", a new family of giant viruses infecting amoebae. Arch. Virol. 158, 915–920.
Dornas, F.P., Rodrigues, F.P., Boratto, P.V., Silva, L.C., Ferreira, P.C., Bonjardim, C.A., Trindade, G.S., Kroon, E.G., La Scola, B., Abrahao, J.S., 2014. Mimivirus circulation among wild and domestic mammals, Amazon Region, Brazil. Emerg. Infect. Dis. 20, 469–472.
Doutre, G., Arfib, B., Rochette, P., Claverie, J.M., Bonin, P., Abergel, C., 2015. Complete genome sequence of a new member of the Marseilleviridae recovered from the brackish submarine spring in the Cassis Port-Miou Calanque, France. Genome Announc. 3.
Doutre, G., Philippe, N., Abergel, C., Claverie, J.M., 2014. Genome analysis of the first Marseilleviridae representative from Australia indicates that most of its genes contribute to virus fitness. J. Virol. 88, 14340–14349.
Erives, A.J., 2017. Phylogenetic analysis of the core histone doublet and DNA topo II genes of Marseilleviridae: evidence of proto-eukaryotic provenance. Epigenetics Chromatin 10, 55.
Fabre, E., Jeudy, S., Santini, S., Legendre, M., Trauchessec, M., Coute, Y., Claverie, J.M., Abergel, C., 2017. Noumeavirus replication relies on a transient remote control of the host nucleus. Nat. Commun. 8, 15087.
Iyer, L.M., Aravind, L., Koonin, E.V., 2001. Common origin of four diverse families of large eukaryotic DNA viruses. J. Virol. 75, 11720–11734.
Klose, T., Kuznetsov, Y.G., Xiao, C., Sun, S., McPherson, A., Rossmann, M.G., 2010. The three-dimensional structure of Mimivirus. Intervirology 53, 268–273.
Klose, T., Reteno, D.G., Benamar, S., Hollerbach, A., Colson, P., La Scola, B., Rossmann, M.G., 2016. Structure of faustovirus, a large dsDNA virus. Proc. Natl. Acad. Sci. USA 113, 6206–6211.
Koonin, E.V., Yutin, N., 2010. Origin and evolution of eukaryotic large nucleo-cytoplasmic DNA viruses. Intervirology 53, 284–292.
Kremer, J.R., Mastronarde, D.N., McIntosh, J.R., 1996. Computer visualization of three-dimensional image data using IMOD. J. Struct. Biol. 116, 71–76.
Kuznetsov, Y.G., Xiao, C., Sun, S., Raoult, D., Rossmann, M., McPherson, A., 2010. Atomic force microscopy investigation of the giant mimivirus. Virology 404, 127–137.
La Scola, B., Audic, S., Robert, C., Jungang, L., de Lamballerie, X., Drancourt, M., Birtles, R., Claverie, J.M., Raoult, D., 2003. A giant virus in amoebae. Science 299, 2033.
Legendre, M., Bartoli, J., Shmakova, L., Jeudy, S., Labadie, K., Adrait, A., Lescot, M., Poirot, O., Bertaux, L., Bruley, C., Coute, Y., Rivkina, E., Abergel, C., Claverie, J.M., 2014. Thirty-thousand-year-old distant relative of giant icosahedral DNA viruses with a pandoravirus morphology. Proc. Natl. Acad. Sci. USA 111, 4274–4279.
Legendre, M., Lartigue, A., Bertaux, L., Jeudy, S., Bartoli, J., Lescot, M., Alempic, J.M., Ramus, C., Bruley, C., Labadie, K., Shmakova, L., Rivkina, E., Coute, Y., Abergel, C., Claverie, J.M., 2015. In-depth study of Mollivirus sibericum, a new 30,000-y-old giant virus infecting Acanthamoeba. Proc. Natl. Acad. Sci. USA 112, E5327–E5335.
Ludtke, S.J., Baldwin, P.R., Chiu, W., 1999. EMAN: semiautomated software for high-resolution single-particle reconstructions. J. Struct. Biol. 128, 82–97.
Monier, A., Larsen, J.B., Sandaa, R.A., Bratbak, G., Claverie, J.M., Ogata, H., 2008. Marine mimivirus relatives are probably large algal viruses. Virol. J. 5, 12.
Nandhagopal, N., Simpson, A.A., Gurnon, J.R., Yan, X., Baker, T.S., Graves, M.V., Van Etten, J.L., Rossmann, M.G., 2002. The structure and evolution of the major capsid protein of a large, lipid-containing DNA virus. Proc. Natl. Acad. Sci. USA 99, 14758–14763.
Perlman, A.J., Stanley, F., Samuels, H.H., 1982. Thyroid hormone nuclear receptor. Evidence for multimeric organization in chromatin. J. Biol. Chem. 257, 930–938.
Pettersen, E.F., Goddard, T.D., Huang, C.C., Couch, G.S., Greenblatt, D.M., Meng, E.C., Ferrin, T.E., 2004. UCSF Chimera–a visualization system for exploratory research and analysis. J. Comput. Chem. 25, 1605–1612.
Philippe, N., Legendre, M., Doutre, G., Coute, Y., Poirot, O., Lescot, M., Arslan, D., Seltzer, V., Bertaux, L., Bruley, C., Garin, J., Claverie, J.M., Abergel, C., 2013. Pandoraviruses: amoeba viruses with genomes up to 2.5 Mb reaching that of parasitic eukaryotes. Science 341, 281–286.
Reteno, D.G., Benamar, S., Khalil, J.B., Andreani, J., Armstrong, N., Klose, T., Rossmann, M., Colson, P., Raoult, D., La Scola, B., 2015. Faustovirus, an asfarvirus-related new lineage of giant viruses infecting amoebae. J. Virol. 89, 6585–6594.
Saadi, H., Reteno, D.G., Colson, P., Aherfi, S., Minodier, P., Pagnier, I., Raoult, D., La Scola, B., 2013. Shan virus: a new mimivirus isolated from the stool of a Tunisian patient with pneumonia. Intervirology 56, 424–429.
Santini, S., Jeudy, S., Bartoli, J., Poirot, O., Lescot, M., Abergel, C., Barbe, V., Wommack, K.E., Noordeloos, A.A., Brussaard, C.P., Claverie, J.M., 2013. Genome of Phaeocystis globosa virus PgV-16T highlights the common ancestry of the largest known DNA viruses infecting eukaryotes. Proc. Natl. Acad. Sci. USA 110, 10800–10805.
Schrad, J.R., Young, E.J., Abrahao, J.S., Cortines, J.R., Parent, K.N., 2017. Microscopic characterization of the Brazilian giant Samba virus. Viruses 9.
Schwartz, Y.B., Kahn, T.G., Pirrotta, V., 2005. Characteristic low density and shear sensitivity of cross-linked chromatin containing polycomb complexes. Mol. Cell. Biol. 25, 432–439.
Simpson, A.A., Nandhagopal, N., Van Etten, J.L., Rossmann, M.G., 2003. Structural analyses of Phycodnaviridae and Iridoviridae. Acta Crystallogr D. Biol. Crystallogr 59, 2053–2059.
Sinkovits, R.S., Baker, T.S., 2010. A tale of two symmetrons: rules for construction of icosahedral capsids from trisymmetrons and pentasymmetrons. J. Struct. Biol. 170, 109–116.
Spahn, C.M., Penczek, P.A., Leith, A., Frank, J., 2000. A method for differentiating proteins from nucleic acids in intermediate-resolution density maps: cryo-electron microscopy defines the quaternary structure of the Escherichia coli 70S ribosome. Structure 8, 937–948.
Tang, G., Peng, L., Baldwin, P.R., Mann, D.S., Jiang, W., Rees, I., Ludtke, S.J., 2007. EMAN2: an extensible image processing suite for electron microscopy. J. Struct. Biol. 157, 38–46.
Thomas, V., Bertelli, C., Collyn, F., Casson, N., Telenti, A., Goesmann, A., Croxatto, A., Greub, G., 2011. Lausannevirus, a giant amoebal virus encoding histone doublets. Environ. Microbiol. 13, 1454–1466.
Van Etten, J.L., Meints, R.H., Kuczmarski, D., Burbank, D.E., Lee, K., 1982. Viruses of symbiotic Chlorella-like algae isolated from Paramecium bursaria and Hydra viridis. Proc. Natl. Acad. Sci. USA 79, 3867–3871.
Vournakis, J., Rich, A., 1971. Size changes in eukaryotic ribosomes. Proc. Natl. Acad. Sci. USA 68, 3021–3025.
Vulovic, M., Voortman, L.M., van Vliet, L.J., Rieger, B., 2014. When to use the projection assumption and the weak-phase object approximation in phase contrast cryo-EM. Ultramicroscopy 136, 61–66.
Wrigley, N.G., 1969. An electron microscope study of the structure of Sericesthis iridescent virus. J. General. Virol. 5, 123–134.
Wu, W., Thomas, J.A., Cheng, N., Black, L.W., Steven, A.C., 2012. Bubblegrams reveal the inner body of bacteriophage phiKZ. Science 335, 182.
Xiao, C., Chipman, P.R., Battisti, A.J., Bowman, V.D., Renesto, P., Raoult, D., Rossmann, M.G., 2005. Cryo-electron microscopy of the giant Mimivirus. J. Mol. Biol. 353, 493–496.
Xiao, C., Fischer, M.G., Bolotaulo, D.M., Ulloa-Rondeau, N., Avila, G.A., Suttle, C.A., 2017. Cryo-EM reconstruction of the Cafeteria roenbergensis virus capsid suggests novel assembly pathway for giant viruses. Sci. Rep. 7, 5484.
Xiao, C., Kuznetsov, Y.G., Sun, S., Hafenstein, S.L., Kostyuchenko, V.A., Chipman, P.R., Suzan-Monti, M., Raoult, D., McPherson, A., Rossmann, M.G., 2009. Structural studies of the giant mimivirus. PLoS Biol. 7, e92.
Yan, X., Chipman, P.R., Castberg, T., Bratbak, G., Baker, T.S., 2005. The marine algal virus PpV01 has an icosahedral capsid with T = 219 quasisymmetry. J. Virol. 79, 9236–9243.
Yan, X., Olson, N.H., Van Etten, J.L., Bergoin, M., Rossmann, M.G., Baker, T.S., 2000. Structure and assembly of large lipid-containing dsDNA viruses. Nat. Struct. Biol. 7, 101–103.
Yutin, N., Koonin, E.V., 2012. Hidden evolutionary complexity of nucleo-cytoplasmic large DNA viruses of eukaryotes. Virol. J. 9, 161.